Self-repairing symmetry in jellyfish through mechanically driven reorganization

Michael J. Abrams[a,1], Ty Basinger[a], William Yuan[b], Chin-Lin Guo[c], and Lea Goentoro[a,1]

[a]Division of Biology and Biological Engineering, California Institute of Technology, Pasadena, CA 91125; [b]Trinity College, University of Oxford, Oxford OX1 3BH, United Kingdom; and [c]Institute of Physics, Academia Sinica, Taipei City 11529, Taiwan, Republic of China

Edited by Clifford J. Tabin, Harvard Medical School, Boston, MA, and approved May 7, 2015 (received for review February 6, 2015)

What happens when an animal is injured and loses important structures? Some animals simply heal the wound, whereas others are able to regenerate lost parts. In this study, we report a previously unidentified strategy of self-repair, where moon jellyfish respond to injuries by reorganizing existing parts, and rebuilding essential body symmetry, without regenerating what is lost. Specifically, in response to arm amputation, the young jellyfish of *Aurelia aurita* rearrange their remaining arms, recenter their manubria, and rebuild their muscular networks, all completed within 12 hours to 4 days. We call this process symmetrization. We find that symmetrization is not driven by external cues, cell proliferation, cell death, and proceeded even when foreign arms were grafted on. Instead, we find that forces generated by the muscular network are essential. Inhibiting pulsation using muscle relaxants completely, and reversibly, blocked symmetrization. Furthermore, we observed that decreasing pulse frequency using muscle relaxants slowed symmetrization, whereas increasing pulse frequency by lowering the magnesium concentration in seawater accelerated symmetrization. A mathematical model that describes the compressive forces from the muscle contraction, within the context of the elastic response from the mesoglea and the ephyra geometry, can recapitulate the recovery of global symmetry. Thus, self-repair in *Aurelia* proceeds through the reorganization of existing parts, and is driven by forces generated by its own propulsion machinery. We find evidence for symmetrization across species of jellyfish (*Chrysaora pacifica*, *Mastigias* sp., and *Cotylorhiza tuberculata*).

self-repair | reorganization | jellyfish | symmetry | propulsion

The moon jelly, *Aurelia aurita*, is one of the most plentiful jellyfish in oceans across the world (Fig. 1*A*). This translucent, saucer-shaped jelly is easily recognizable by the four crescent-shaped gonads on its umbrella. The moon jelly varies greatly in size, from a few inches to a foot (1–3). Ranging from tropical seas to subarctic regions, from the open ocean to brackish estuaries, the moon jelly occupies diverse habitats (4–6). It can even thrive in dirty, polluted, acidified, warm, and oxygen-poor waters (7–10). Presently, jelly blooms have been increasing in size and frequency worldwide, which has been interpreted as a troubling sign of a disturbed ocean ecosystem (11, 12).

Aurelia belongs to the class Scyphozoa, of the ancient phylum Cnidaria, which includes corals, hydras, siphonophores, and box jellyfish (13, 14). Cnidarians are unified by common characteristics, such as radial symmetry, dipoblasticity, diffuse nerve nets, mesoglea, and the stinging cells, or cnidocytes, which give the group its name. *Aurelia*, and many other Scyphozoan jellyfish, have a dimorphic life cycle with two adult forms: the sexually reproducing, free-swimming medusa, and the asexually reproducing, sessile polyp (Fig. 1*B*). Fertilized eggs develop into ciliated planulae that settle and mature into polyps. The polyps reproduce asexually through budding, or metamorphose and strobilate to produce juvenile jellyfish, called ephyrae. The ephyrae mature into medusae as bell tissues grow between the arms and reproductive structures develop. Transition into medusa may proceed over 1 mo in the laboratory (with abundant feeding), or longer in the wild. The ephyra stage is hardy and can withstand months of starvation (15).

Injury is common in marine invertebrates. Examining 105 studies, Lindsay (16) showed that, at any given time, about 33–47% of the benthic fauna is injured. Some cited studies recorded entire starfish populations with at least one injured arm. Injury may be due to numerous factors, including partial predation, autotomy, cannibalism, competitive interaction, and human activities. Jellyfish have many known predators. A well-studied group of predators are the sea turtles (e.g., the leatherback and the loggerhead; Fig. 1*C*). Juvenile sea turtles have been observed biting into foot-wide jellyfish, and adults gorge on an average of 261 jellyfish per day (12). In addition, over 124 species of fish, 11 species of birds, several species of shrimps, sea anemones, corals, and crabs are reported to assail *Aurelia* (17–20). Barnacles have been reported to catch and digest newly strobilated ephyrae (21).

Here, we ask how *Aurelia* responds to injuries. Marine invertebrates are known for their regenerative ability. Reported cases of regenerating marine organisms include jellyfish, sponges, corals, ctenophores, sea anemones, clams, polychaetes, starfish, and brittlestars (14, 16, 22–26). Isolated striated muscle from hydromedusae can transdifferentiate to regenerate various cell types (27). The polyps of *Aurelia*, and a number of other species, can regenerate tentacles, stolonts, and hydrants (28–31), and an entire polyp can regrow from a single polyp tentacle (32). In this study, we investigated the repair capacity in the free-swimming forms of *Aurelia* and discovered that *Aurelia* have evolved a fast strategy of self-repair, one that does not involve regenerating lost body parts.

Results

To study how the free-swimming forms of *Aurelia* respond to injuries, we chose to examine the ephyrae, the discrete symmetry of

Significance

Animals are endowed with the capacity to repair injuries. In this study, we found that, upon amputation, the moon jellyfish *Aurelia aurita* rearranges existing body parts and recovers radial symmetry within a few days. This unique strategy of self-repair, which we call symmetrization, requires mechanical forces generated by the muscle-based propulsion machinery. We observed a similar strategy in a number of other jellyfish species. This finding may contribute to understanding the evolutionary pressures governing biological self-repair strategies. Beyond biology, this finding may inspire a mechanically driven, self-organizing machinery that recovers essential geometry without regenerating precise forms.

Author contributions: M.J.A., T.B., and L.G. designed research; M.J.A. and T.B. performed experiments; W.Y. performed the grafting experiments; M.J.A., C.-L.G., and L.G. designed the mathematical model; C.L.G. performed the mathematical modeling; M.J.A., T.B., and L.G. analyzed data; and M.J.A., T.B., and L.G. wrote the paper.

The authors declare no conflict of interest.

This article is a PNAS Direct Submission.

Freely available online through the PNAS open access option.

[1]To whom correspondence may be addressed. Email: goentoro@caltech.edu or mabrams@caltech.edu.

This article contains supporting information online at www.pnas.org/lookup/suppl/doi:10.1073/pnas.1502497112/-/DCSupplemental.

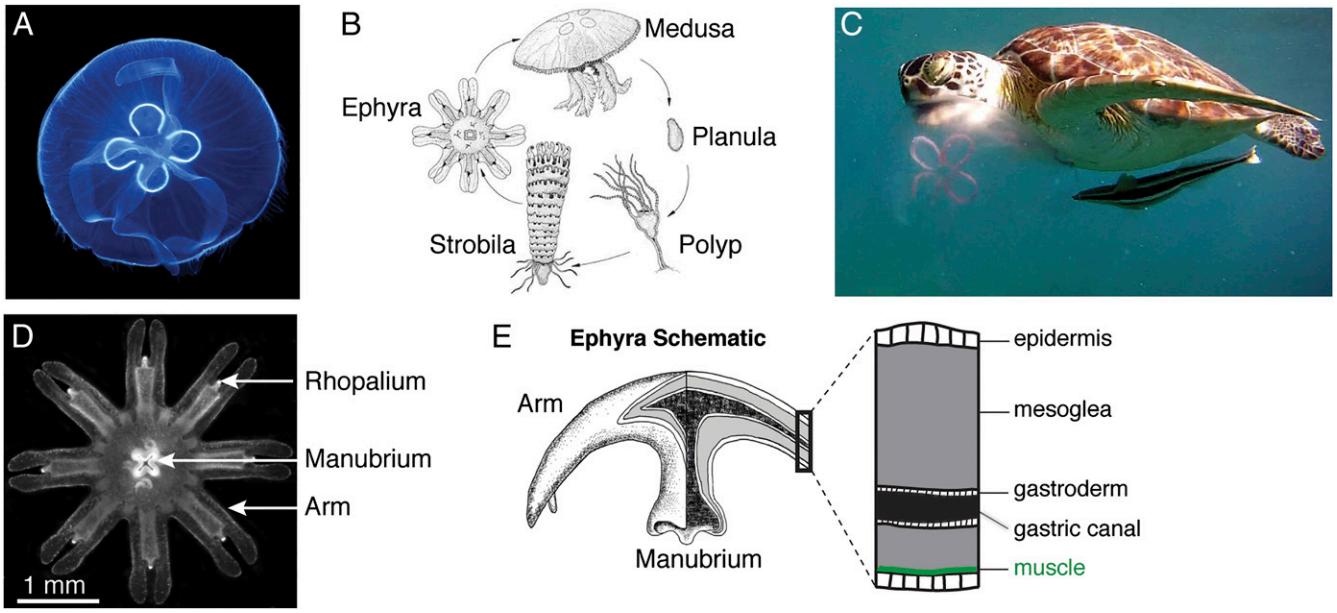

Fig. 1. Life cycle and anatomy of *Aurelia aurita*. (*A*) Adult *Aurelia*. The blue color is due to lighting. Image courtesy of Wikimedia Commons/Hans Hillewaert. Image © Hans Hillewaert. (*B*) *Aurelia* life cycle. Fertilized eggs develop into larval planulae, which settle and develop into polyps. Seasonally, or in the right conditions, the polyps metamorphose into strobilae and release free-swimming, juvenile jellyfish (a process called strobilation). The young jellyfish, called ephyrae, grow into medusae in 3–4 wk. Reprinted with permission from ref. 13. (*C*) A juvenile green sea turtle preying on *Aurelia* at Playa Tamarindo, Puerto Rico. Image courtesy of R. P. van Dam. (*D*) An *Aurelia* ephyra has eight radially symmetrical arms, surrounding the manubrium at the center. At the end of each arm is a light- and gravity-sensing organ, called rhopalium. (*E*) The epithelium of ephyra is composed of two cell layers, the ectoderm-derived epidermis that faces the outer side and the endoderm-derived gastrodermis that lines the gastric cavity. Between the two layers is the gelatinous, viscoelastic mesoglea. Embedded in the subumbrellar side (mouth side) is the coronal muscle (green).

which gave us clear morphological markers to follow (Fig. 1*D*). Newly strobilated ephyrae are typically 3–5 mm in diameter (Movie S1). They have a disk-shaped body, with eight symmetrical arms. Also called lobes, lappets, or tentaculocytes by other authors, these arms form a swimming apparatus in the ephyrae. Viscous boundary layers of fluid form between the arms to create a hydrodynamically continuous paddling surface (33). Symmetric pulsation of the arms generates fluid flow that facilitates propulsion and prey capture (34, 35). As ephyrae grow into medusae, bell tissues grow between the arms, replacing a viscous bell with a physical one.

At the end of each arm is a sensory organ, called rophalium, which contains ocelli, chemosensory pits, and a statocyst (14). At the center of the body is the manubrium, a muscular channel connecting the mouth to the gastrovascular cavity. The stomach is surrounded by an epithelium composed of two cells layers, the outer-facing epidermis (containing the stinging cells) and the gastrodermis lining the stomach (Fig. 1*E*). Between the two cells layers is the mesoglea, a viscoelastic, jelly-like substance composed predominantly of fibrous proteins and water (36).

We conducted the amputation experiments in the following way. Freshly strobilated ephyrae were anesthetized and amputated using a homemade razor knife (Fig. 2*A* and *Materials and Methods*). Ephyrae were immediately returned to artificial seawater (ASW) to recover. Muscle contractions typically resumed within minutes. Fig. 2 *B* and *C* shows a typical progression of recovery. The three-armed and five-armed pieces here were cut from an individual ephyra. The process commenced within minutes. The wound at the cut site closed within the first hours. The arms gradually spread further apart, as the manubrium relocated to the center of the body. Within 18 h in this experiment, we observed fully symmetrical three-armed and five-armed ephyrae.

We call this process "symmetrization" to denote the recovery of radial symmetry, rather than regeneration of precise initial body parts, e.g., the missing arms. Symmetrization was observed across amputation schemes. Fig. 2*D* shows symmetrical ephyrae that recovered from injury with two, three, four, five, six, and seven arms. Symmetrization even proceeded in grafting experiments: a foreign arm grafted onto a cut tetramer led to the formation of a fivefold symmetrical ephyra (Fig. S1).

Symmetrization occurred at high frequency (Fig. 2*E*). We amputated hundreds of ephyrae and observed frequency of symmetrization ranging from 72% to 96% across amputation schemes. In the ephyrae that did not symmetrize, the cut wounds simply closed, with little traces of the initial injury. The speed of recovery varied, but ephyrae typically symmetrized within 12 h to 4 d (Fig. 2*F*).

We tested whether ephyrae that regained radial symmetry could continue developing. Two- and three-armed ephyrae, which have no manubrium for feeding, did not develop further, and typically died within 2 wk. We observed pronounced effects in ephyrae with four to six arms. Ephyrae that reformed symmetry matured into medusae; developed gonads, full bells, and oral arms (Fig. 2*E*; $n = 19$); and showed active swimming (Movie S2). Ephyrae that remained asymmetrical developed shrunken bells and disproportionately large manubria (Fig. 2*F*; $n = 10$), and remained sunken at the bottom of the aquaria (Movie S2). These results suggest that regaining radial symmetry facilitates further development of injured ephyrae into adult medusae.

Interestingly, radially symmetrical nonoctamers have been observed in *Aurelia* populations in the wild (37–40), as well as cited by William Bateson (41) as an example of meristic variation, and they are not rare. Scoring freshly strobilated ephyrae, we observed that 9.5% of the ephyrae in our laboratory population are nonoctamers (Fig. 3*A*), consistent with a previous study in marine aquaria (42). The natural nonoctamers range from having 4 to 16 arms and are capable of maturing into medusae. These natural nonoctamers look indistinguishable from those recovering from the amputation experiments (Fig. 3*B*). Furthermore, we found that, in ephyrae, the body size scales with the number of arms and that this scaling is conserved between the natural and the

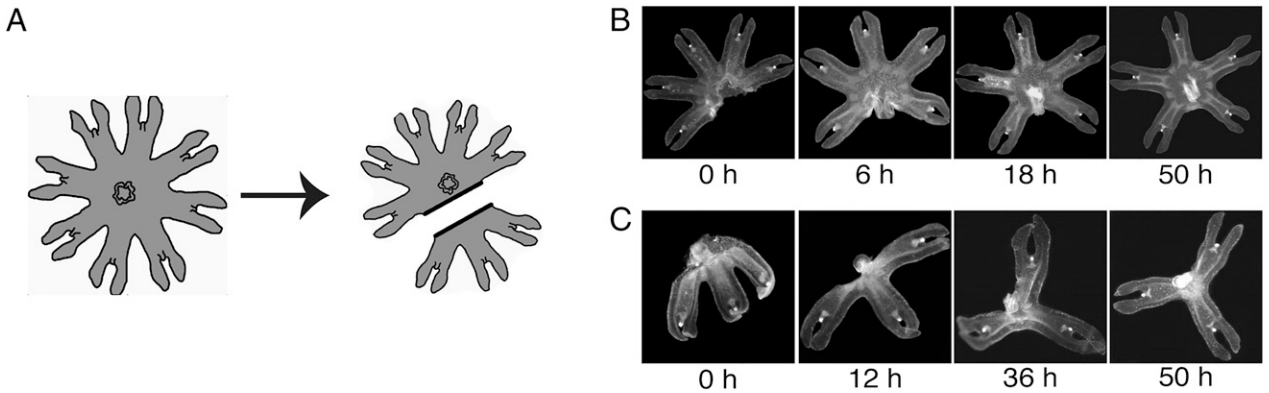

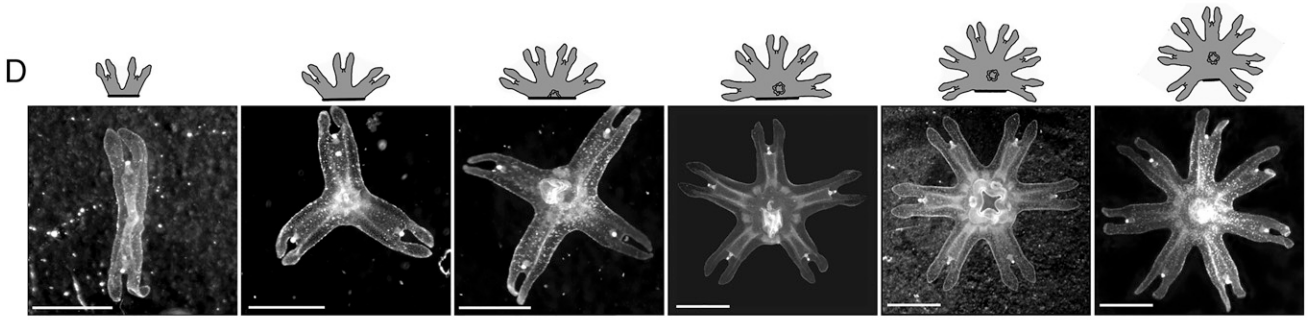

E

Number of Arms	Fraction that Symmetrized	Percentage
Two	45/50	90.0
Three	31/43	72.1
Four	150/160	93.8
Five	125/130	96.2
Six	75/82	91.2
Seven	32/34	94.1

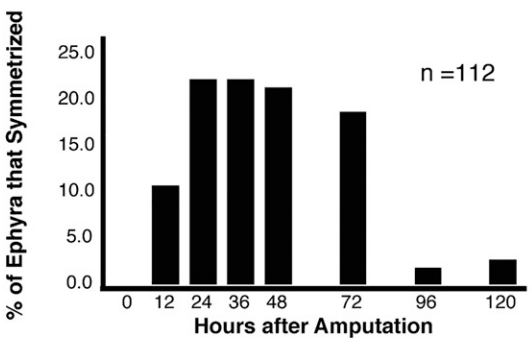

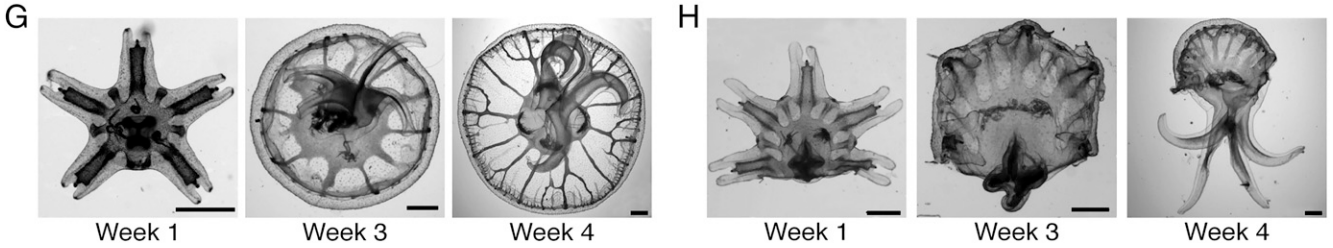

Fig. 2. *Aurelia* ephyra reorganize existing arms to regain radial symmetry. (*A*) An example of amputation schemes used in the study. Cuts were performed across the body using a razor blade. (*B* and *C*) A three-armed and five-armed piece amputated from a single ephyra. Within 2 d, neither regenerated the lost arms. Instead, each reorganized to reform radial symmetry. (*D*) Symmetrization was observed with two, three, four, five, six, and seven arms. The cartoons indicate the initial forms after amputation. (*E*) Percentage of symmetrization across amputation schemes. The ephyrae in the amputation experiments were 1–3 d old (after strobilation) and were examined daily for 4 d. (*F*) Progression of symmetrization. In this experiment, we counted the number of ephyrae that symmetrized at the indicated time. Data were collected from dimers, tetramers, pentamers, and hexamers. There is a slight trend in the recovery speed across amputation scheme. The 12-h recovery is typical for dimers. Symmetrical tetramers and pentamers often started appearing by day 1 onward, as analyzed in more detail in Fig. 5*H*. (*G* and *H*) Ephyrae in these experiments were tracked individually for 1 mo, fed daily, and imaged every 2–3 d. (*G*) Pentamers that symmetrized continued growing into mature medusa ($n = 19$). (*H*) Pentamers that did not symmetrize grew abnormally with oversized manubria ($n = 10$). (Scale bar in each photograph: 1 mm.)

amputated ephyrae (Fig. 3*C*). The conserved scaling is remarkable because the ephyrae were simply cut in the amputation experiments and the amount of body lost was variable, suggesting an active geometric regulation. These results show that symmetrization produces physiologically relevant morphologies, recapitulating those generated by developmental variation.

Next, we investigated the mechanism that drives the recovery of radial symmetry. We did not find obvious requirement for global external input. Symmetrization proceeded in stagnant or moving water, in light or dark, and even when the ephyrae were pinned upside down. Symmetrization also occurred when the ephyrae were reared alone or in groups. Neither did we see an

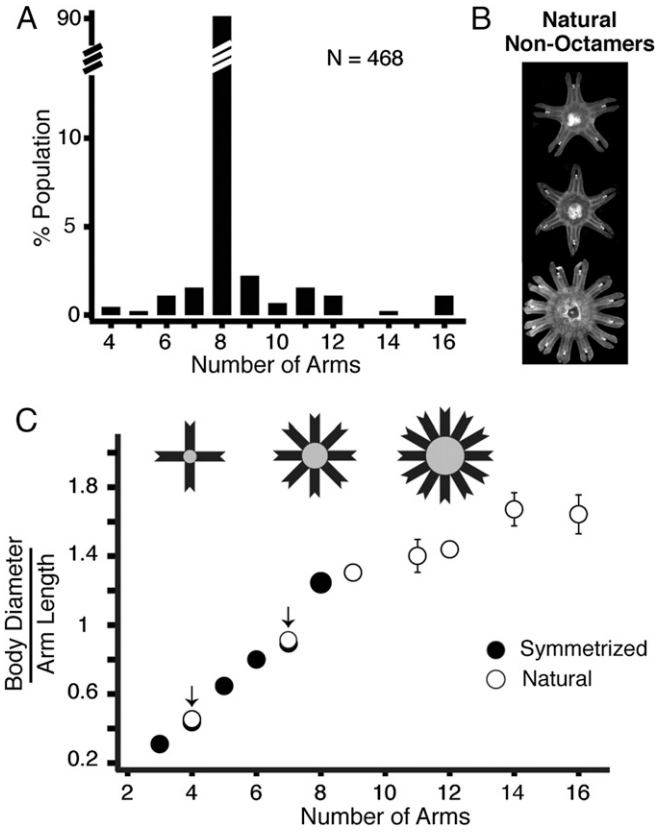

Fig. 3. Symmetrization phenocopies developmental variation. (*A*) Non-octamers form 9.5% of the *Aurelia* population in our laboratory. Ephyrae were scored immediately upon strobilation. This histogram come from multiple strobilae in a single strobilation round. A single strobila may produce 10–20 ephyrae, with variable numbers of arms. (*B*) A natural pentamer, hexamer, and dodecamer. (*C*) White circles: body size of natural ephyrae. Black circles: body size of ephyrae from symmetrization. Both plotted as a function of the arm number. The arrows indicate where there are both black and white circles overlapping. Body size was measured as the diameter (the gray region in the ephyra cartoons). We normalized body diameter to arm length (black regions of the ephyra cartoons), to account for variation across ephyrae. The ephyrae also grew in size over time; to account for this, we characterized the growth curve and normalized all measurements to 1-d-old ephyrae (*Materials and Methods*). A total of 46 ephyrae was measured to generate this plot. Error bars are SD from more than three ephyrae. Some error bars are not seen because they are smaller than the circles.

obvious global organizer within the body. As Fig. 2*C* shows, ribbons of two or three arms, missing the majority of the central body, recovered symmetry. Finally, symmetrization is not simply driven by wound closure. The wound closed within hours, preceding symmetry reformation. Moreover, the wound also closed in amputated ephyrae that did not symmetrize.

We next investigated other classes of mechanisms that could explain symmetrization. One possibility was that symmetrization might be driven by localized cell proliferation that could push the arms apart (Fig. 4*A*). Local cell proliferation in the *Drosophila* wing disk can generate global tension that rapidly drives changes in tissue shape (43, 44). To mark cell proliferation, we used 5-ethynyl-2′-deoxyuridine (EdU), a thymidine analog that gets incorporated into newly synthesized DNA (45). Fig. 4*B* shows EdU staining in the cut tetramers with no obvious localized patterns (the green EdU stain here reflects the cumulative DNA synthesis over 4 d). We saw similar staining in the uncut ephyrae (Fig. S2). Denser stain was seen in the manubrium (circled) and rophalia. Moreover, when we blocked cell proliferation using 20 μM hydroxyurea, the EdU stain was largely abolished (Fig. 4*C*), and symmetrization progressed fully, and at a normal pace ($n = 40$). We observed the same results using another inhibitor of cell proliferation, 5-fluoroacil (10 μM; $n = 40$).

Alternatively, symmetrization may be driven by localized cell death, creating a negative pressure space that pulls the arms around the body (Fig. 4*D*). Apoptosis in *Drosophila* embryogenesis can produce forces that pull in neighboring cells (46). We assessed cell death using Sytox, a DNA-binding dye that does not cross intact cell membranes and therefore only stains cells with compromised membranes, a proxy for dying cells. As a positive control, we saw high Sytox stain when we fixed the ephyrae (hence permeabilizing all cells), and when we treated the ephyrae with an apoptosis inducer (100 nM gambogic acid; Fig. S2; $n = 19$ of 20). Fig. 4*E* shows that there was little staining in the cut tetramers. We saw similarly little stain in uncut ephyrae (Fig. S2). We stained every 24 h after amputation and did not see an increase in Sytox staining during symmetrization. High Sytox stain was seen in the manubrium and rophalia; both are regions of high EdU staining, indicating these are areas of high cell turnover. Finally, when we treated the ephyrae with a caspase inhibitor (100 μM Z-vad-fmk), the Sytox stain was largely reduced (Fig. 4*F*, $n = 17$ of 20), and still symmetrization progressed normally.

Thus, neither cell proliferation nor cell death seems to play a significant role in driving the recovery of body symmetry. Symmetrization appears to be primarily driven by the reallocation of existing cells and tissues. What might be other sources of force that could mediate rebalancing of existing body parts? A prominent structure in the ephyrae is the striated musculature network (14, 47, 48). Phalloidin staining in Fig. 4*G* shows actin enriched in the muscle, revealing the axisymmetric architecture of the ephyra musculature, with a coronal ring in the central body, and radial rays extending into each arm. Fig. 4*H* shows a freshly cut tetramer, where the halved manubrium and the blunt muscle ends can be seen at the edge of the wound. Fig. 4*I* show how the ends of the coronal muscle gradually extended toward each other as the ephyrae symmetrized (see arrows), and reconnected to reform axisymmetrical musculature (Fig. 4*J*).

We asked whether the musculature network plays a role in symmetrization. First, we tested the idea that perhaps the muscle reconnection itself pulls the arms along into symmetrical positions (Fig. 4*K*). To block muscle reconnection, we treated the cut ephyrae with cytochalasin D, which inhibits actin polymerization. Pretreatment with cytochalasin D (for 1 d before amputation) blocked the wound closure, and the ephyrae died. This suggests that wound closure requires actin dynamics and that wound closure is a necessary first step in symmetrization, even though it does not drive symmetrization because the wound also closes normally in unsymmetrized ephyrae. To avoid the lethal effects, in subsequent experiments, ephyrae were amputated first and then immediately incubated in cytochalasin D. Treated ephyra continued pulsing and feeding (as also observed in ref. 49), and the wound closed normally. At high doses of cytochalasin D (2 μM), the vast majority of ephyrae failed to symmetrize (Fig. 4*L*; $n = 66$ of 76). Similar effects were observed with other actin inhibitors, dihydro-cytochalasin B ($n = 20$ of 20) at 750 nM and latrunculin A at 60 nM ($n = 19$ of 20).

The lower dose, however, is more revealing. At 500 nM, cytochalasin D treatment blocked reconnection of the coronal muscle (Fig. 4*N*), despite which the ephyrae often symmetrized ($n = 14$ of 21). In fact, we also observed this with 2 μM cytochalasin D, but at a lower percentage (Fig. 4*M*; $n = 10$ of 76). Muscle reconnection therefore does not fully explain symmetrization, because ephyrae could symmetrize normally without it. We seem to have disentangled two effects here. The higher doses of cytochalasin D may reveal the more nonspecific effects on actin cytoskeleton beyond the muscle cells, possibly suggesting a role for actin dynamics in tissue repositioning [as has been

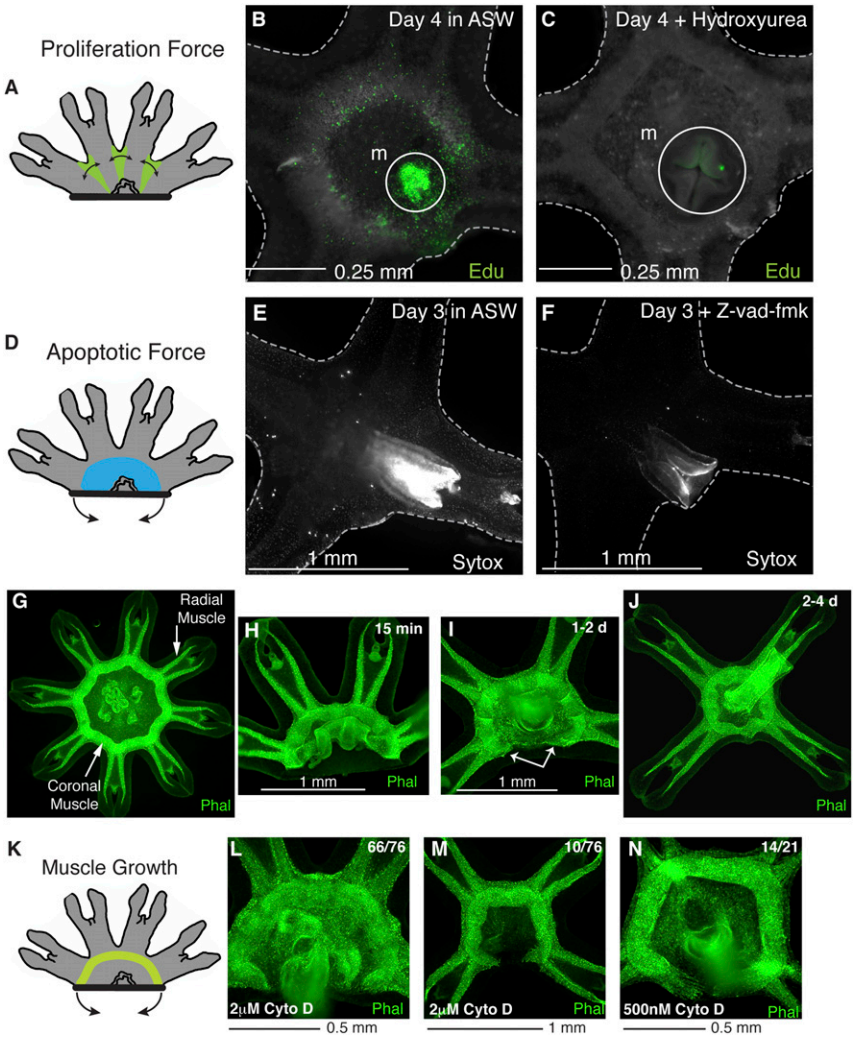

Fig. 4. Symmetrization is not driven by cell proliferation, cell death, or muscle reconnection. (*A–D*) Is symmetrization driven by cell proliferation? (*A*) Localized cell proliferation (e.g., in the green regions) may push the arms apart. (*B*) EdU stain (green) in a symmetrized tetramer, showing cumulative signal over 4 d. (*C*) EdU stain was abolished in the presence of 20 μM hydroxyurea. In this experiment, the cut ephyrae were incubated in EdU with or without 20 μM hydroxyurea for 4 d. The solution was refreshed daily. Ephyrae were fixed and stained on day 4 (*Materials and Methods*). (*D-F*) Is symmetrization driven by cell death? (*D*) Localized cell death (e.g., in the blue region) may pull the arms into the cut site. (*E*) Sytox stain (white) in a symmetrized ephyra 3 d after amputation. (*F*) Sytox stain was abolished in the presence of a caspase inhibitor (100 μM Z-vad-fmk). Cut ephyrae were incubated in the inhibitor for 3 d, and then stained with Sytox (*Materials and Methods*). (*G–J*) Symmetrization is accompanied by reconnection of coronal muscle. (*G*) Staining of the musculature in an uncut ephyra. Muscle was visualized using phalloidin–Alexa Fluor 488 (*Materials and Methods*). (*H–J*) Staining of muscle in symmetrizing ephyrae. Ephyrae were fixed and stained at 15 min (*H*), 1 d (*I*), and 3 d after amputation (*J*). White arrows in *K* indicate the extending edges of the muscle. (*K–N*) Is symmetrization driven by muscle reconnection? (*K*) Reconnection of muscle (green) may pull the arms along. (*L–N*) Ephyrae were amputated, incubated in 2 μM (*L–M*) or 500 nM (*N*) cytochalasin D for 4 d, and then stained with phalloidin–Alexa Fluor 488.

proposed in other systems (50, 51)]. The lower doses of cytochalasin D showed that actin polymerization is necessary for the reconnection of the coronal muscle but that this can be decoupled from, and more importantly does not drive, symmetrization.

To determine forces upstream of muscle reconnection, we turned to the muscle function itself. The jellyfish muscle network generates contractile forces that drive bell pulsation. This generates fluid flow that facilitates propulsion and prey capture (33–35, 52). Muscle filaments are located in the basal extension of the epitheliomuscular cells, embedded in the subumbrellar mesoglea, and receive inputs from the surrounding diffuse nervous systems and ganglionic pacemakers (14, 53). To inhibit muscle contraction, we tested a number of muscle relaxants that were soluble in seawater (e.g., tricaine, bezoncaine, urethane), and most of them were fatal within a day. However, two muscle relaxants, menthol and magnesium chloride, proved to be gentle enough: the ephyra remained alive in the anesthetics for >3 wk. Both anesthetics have been used in a number of studies in marine invertebrates (54–56) and are thought to modulate the excitation–contraction coupling by blocking voltage-gated ion channels (57, 58) that transmit electrical stimuli to the muscle.

In 400 μM menthol, all treated ephyrae were motionless and failed to symmetrize (Fig. 5*A*; $n = 60$ of 60). The arms remained asymmetrical, the manubrium remained at the edge, and the cut muscle remained blunt (Fig. 5*B*). The effect was reversible: ephyrae removed from menthol resumed symmetrization (Fig. 5*C*; $n = 20$ of 20). We observed the same complete inhibition of symmetry recovery with 2.5% (wt/vol) $MgCl_2$ ($n = 20$ of 20). Because motionless ephyrae could not feed effectively, we confirmed that all control-starved ephyrae symmetrized appropriately ($n = 20$ of 20). Thus, inhibiting muscle contraction completely blocked symmetrization. This argues that forces generated by muscle contraction during pulsation are necessary for symmetrization.

How might forces from muscle contraction drive the recovery of radial symmetry? To understand this, we consider muscle contraction in the context of its roles in propulsion. A stroke cycle in jellyfish consists of alternating fast muscle contraction (the power stroke), followed by a slow elastic response from the gelatinous mesoglea (the recovery stroke) (Fig. 5*D*; Movie S1 shows an ephyra swimming in seawater) (52, 59, 60). Activation of the axisymmetric musculature produces symmetric bell contraction and a forward thrust. Recovery stroke, powered by the elastic aspects of the mesoglea, brings the bell to its original shape and generates a secondary thrust in the process. In ephyra, where there are discontinuous arms, a continuous paddling surface is generated by viscous, overlapping boundary layers between the symmetrically arranged arms (33).

In such an interlinked system where the symmetry of the arm and muscle architecture is essential for driving propulsion, loss of symmetry would be immediately sensed through imbalance in the interacting forces. In uncut ephyrae, muscle contraction produces an axisymmetric compression that is balanced in all directions. In amputated ephyrae, where the geometric balance is disrupted, the asymmetrical compression from muscle contraction, followed by the elastic response, may intuitively produce a net angular pivoting of the arms into the cut site, where there is less opposing bulk (Fig. 5*D*). This is akin to squeezing an elastic ball at one end

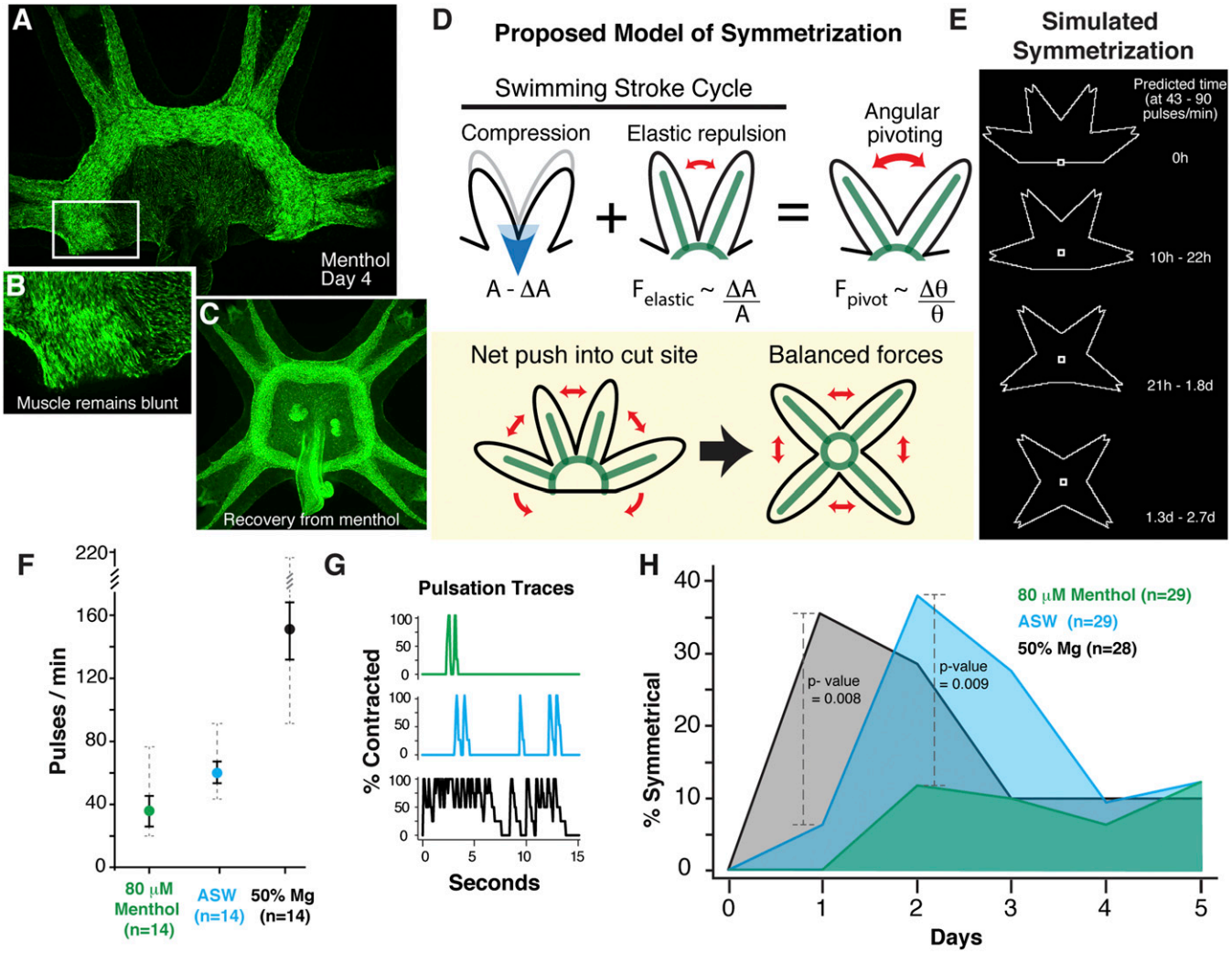

Fig. 5. Symmetrization is driven by muscle contraction in the propulsion machinery. (*A–C*) Inhibiting muscle contraction blocks symmetrization. (*A*) Amputated ephyrae were incubated in 400 μM menthol for 4 d, and then stained with phalloidin. All treated ephyrae failed to symmetrize ($n = 60$ of 60). (*B*) A magnified view shows that the cut muscle remained blunt in the presence of menthol. (*C*) Ephyrae removed from menthol (after 4 d) resumed and completed symmetrization within 4 d ($n = 20$ of 20). (*D* and *E*) Proposed model of symmetrization. (*D*) A swimming stroke consists of muscle contraction, which generates compression, followed by elastic response from the mesoglea. We propose that, in the amputated ephyrae, this leads to angular pivoting into the cut site, as there is less bulk resistance. With repeated cycles of compression and elastic repulsion, the arms gradually relax into a more symmetrical state, until the forces are rebalanced. (*E*) Mathematical simulation of the symmetrization of a tetramer, taking into account the compression generated by the muscle contraction, the elastic response, and the ephyra geometry (see *Supporting Information* for details of the model). The predicted time of symmetrization is computed based on the pulsation frequency measured in seawater (Fig. 5*F*). (*F–H*) Frequency of muscle contraction dictates the speed of symmetrization. (*F*) Incubation in reduced $MgCl_2$ (50% of the normal seawater) increased the frequency of muscle contraction, whereas incubation in 80 μM menthol decreased the frequency of muscle contraction. The dashed gray line shows the full range of the data, whereas the black lines indicate 95% confidence intervals. (*G*) Sample traces of ephyra pulsation in normal seawater (blue), reduced magnesium (black), and 80 μM menthol (green). Frequency of muscle contraction was counted by hand from time-lapse movies taken at 15 fps. A single pulse typically takes 0.5 s. Full contraction was when the ephyrae fully closed in, and partial contraction was when the arms only contracted halfway. (*H*) Cut ephyrae were incubated in normal seawater (blue), seawater with reduced $MgCl_2$ (black), or 80 μM menthol (green), and scored every day for symmetrization.

and producing a protrusion on the other side. With each cycle of compression and elastic repulsion, the arms may then relax to a new stable state. Through repetition of this cycle, the arms may gradually ratchet into the cut site, until the morphology is geometrically rebalanced (Fig. 5*D*).

To test this intuitive model, we built a mathematical model that considers forces generated by the muscle contraction and the mesoglea elastic response, in the context of ephyra geometry (detailed in *Supporting Information* and Fig. S6). The dimensions of the ephyrae were measured directly, and the elastic and tensile modulus of the body were obtained from previous biomechanic studies (36, 61). Simulation of the model (Fig. 5*E* and Movie S3) shows that interactions between these local forces can indeed recover global symmetry. Not only does the model recapitulate the symmetry recovery but it also captures the timescale of symmetry recovery, predicting a recovery time of 1.3–2.7 d (see Fig. 5*E* and *Supporting Information* for detailed calculation). The force–balance model makes a prediction: the speed of symmetrization is proportional to the frequency of muscle contraction. If the ephyrae pulse more often, they will symmetrize faster.

To test the model prediction, we use gentle perturbations to modulate the frequency of muscle contraction in the ephyrae. Muscle contraction can be stimulated by reducing magnesium concentration in seawater, as was also observed in ref. 62. Fig. 5 *F–H* shows that a 50% reduction in magnesium ions (referred to as "reduced Mg") increased the frequency of contraction in ephyrae (shown in black; also see Movie S4, with the control in Movie S4). Under this increased frequency of muscle contraction, symmetrization proceeded faster (Fig. 5*H*; $n = 28$). Within a day, 36% of ephyrae in reduced Mg symmetrized, higher than the 7% in ASW (P value < 0.01). In the parallel experiment, we slowed down muscle contraction by treating ephyrae with 80 μM menthol. Under this condition, the ephyrae pulsed less frequently (shown in green in Fig. 5 *F–H* and Movie S4) and symmetrized more slowly (Fig. 5*H*; $n = 29$). By day 2, only 14% of ephyrae symmetrized in 80 μM menthol, compared with 38% in ASW (P value < 0.01). As predicted by the model, the speed of symmetrization indeed correlates with the frequency of muscle contraction. Higher frequency of muscle contraction delivers more work per unit time and drives faster symmetrization.

Moreover, the simple model captures the orders of magnitude of the observed symmetrization time. In reduced Mg, they pulse 92–215 per min (Fig. 5*F*), which predicts a symmetrization time of 13 h to 1.25 d (see *Supporting Information* for detailed calculation). This corresponds nicely with the observed peak at day 1 in reduced Mg (Fig. 5*H*). In 80 μM menthol, they pulse 20–76 per min (Fig. 5*F*), which the model predicts would have a symmetrization time of 1.5–5.8 d, corresponding to the broad spread we see in the menthol experiment (Fig. 5*H*).

The correlation between pulsation rate and symmetrization speed supports the idea that muscle contraction plays a dominant role in driving symmetrization. One potential caveat here is that menthol and magnesium may also affect ion flow in nonmuscle cells. To further confirm the specific role of muscle contraction, we used two different inhibitors of skeletal muscle myosin II, *N*-benzyl-*p*-toluene sulfonamide (BTS) and 2,3-butanedione monoxime (BDM) (63, 64). Similar to those treated with menthol and reduced Mg, the myosin-inhibited ephyrae were also incapable of pulsing and survived for over a week in the treatment. We saw no symmetrization in ephyrae incubated in 150 μM BTS ($n = 40$ of 40) or 25 mM BDM ($n = 40$ of 40), as shown in Fig. S3. Examining phalloidin staining in these ephyrae showed blunt coronal muscle on the cut edge, indistinguishable from those incubated in 400 μM menthol (compare Fig. S3 to Fig. 5).

Finally, might recovering symmetry, rather than precise body parts, be a more general strategy across Scyphozoa? The Scyphozoa class in Cnidaria encompasses some 200 extant species, the majority of which undergo an ephyra stage. Despite the morphological diversity of the adult medusae, the ephyrae across species are incredibly similar, in anatomy, in musculature, and in size (most known ephyrae range between 3 and 5 mm; ref. 38). Indeed, we observed symmetrization in *Chrysaora pacifica*, *Mastigias* sp., and *Cotylorhiza tuberculata* (Fig. S4). Halved ephyrae of these species did not regenerate lost arms, but reorganized and regained radial symmetry within 1–4 d. Together with our observations in *Aurelia*, this suggests that symmetrization is present across two major orders of the Scyphozoa (order Semaeostomeae and Rhizostomeae).

Discussion

We describe in this study a strategy of self-repair in jellyfish, where, in response to severe injuries, *Aurelia* ephyrae do not regenerate lost parts or simply close the wound; rather, the organisms reorganize existing parts and recover body symmetry. The absence of regeneration of arms is interesting in light of the fact that *Aurelia* is capable of regeneration—*Aurelia* polyps can regenerate from a single polyp tentacle (32). It appears that rapidly regaining body symmetry, rather than precise body parts, may be more critical in the free-swimming ephyrae.

Radial symmetry in jellyfish is essential for propulsion, and it is interesting that the propulsion machinery intrinsically facilitates both sensing the loss of symmetry, and the repair of symmetry. Symmetrization does not require making new cells or losing cells through programmed death. Instead, it is clear from our work that mechanical forces play the dominant role in this self-repair process. Rather than activating a special module, self-repair in jellyfish uses constitutive physiological machinery. It will be interesting next to investigate the molecular underpinnings that transmit forces from muscle contraction into tissue reorganization. Our data indicate the roles of actin polymerization. As mechanical forces and cytoskeletal dynamics are increasingly implicated in morphogenesis, symmetrization in *Aurelia* with discrete geometry, clear morphological readout, and amenability to molecular tools, may emerge as a model system for probing such questions. Moreover, we observed that a given polyp generated ephyrae with a variable number of arms. It will be interesting to investigate whether mechanical forces play a role during development to maintain symmetry and facilitate the generation of natural variation.

The lack of an increase in cell proliferation during symmetrization partially brings to mind morphallaxis in hydra, in which lost structures are regenerated without increase in cell proliferation (25, 65–67). Our study therefore suggests a potentially interesting pattern: there are now two repair strategies without increased cell proliferation in Cnidaria, one to restore lost parts (in hydra) and another to restore functional symmetry without restoring lost parts (in *Aurelia*).

Two points have not been explicitly addressed in our model. First, the ratchet aspect of symmetrization. Over hours or days, the arms gradually move into the cut site, until symmetry is fully regained. The mesoglea is a viscoelastic material that produces an elastic response over short timescales but behaves like a viscous fluid over longer time periods (36, 61, 68, 69). Therefore, the ephyrae behaves like an elastic object in responding to fast muscular compression, and we speculate that the viscous aspect of the mesoglea may then help relax the organism to a new state with the arms slightly repositioned into the cut site. Symmetrization relies as much on the force-generating muscle machinery as on the material properties of the reorganized tissues. Second, it is striking that, in all of our amputation experiments, the recovering ephyrae remained planar. One way we successfully broke planarity was by removing the manubrium altogether. These ephyrae recovered to a bilaterally symmetrical fan shape (Fig. S5*A*), or a spiral shape (Fig. S5*B*). The manubrium, lined with muscle and connected to the body through a dense actin-rich network, may plausibly act as a source of rigid planarity.

Our study suggests a different framework to reinterpret previously reported lack of regeneration in other marine invertebrates.

In Hydrozoa, Hargitt suggested in 1897 that injured hydromedusae (*Gonionemus vertens*) did not regenerate but instead recast themselves into "a morphological equivalent of their original form" (70). In Ctenophores, Coonfield noted in 1936 that, although ~50% of ctenophores (*Mnemiopsis* sp.) regenerated after quartering, the other 50% did not regenerate but rather "rounded up and behaved as normal animals" (71). Our work establishes the lack of regeneration in Scyphozoa, demonstrates reorganization to recover body symmetry as an active process that facilitates growth and development, and presents the underlying mechanism. Symmetrization is an agile strategy: it proceeds from various starting conditions, it uses constitutive physiological machinery, and it is fast and plausibly energy conserving (as it does not require new cells). It will be interesting to test whether symmetrization has evolved as a parallel or alternative strategy to regeneration across radially symmetrical animals.

Finally, beyond biology, the finding of a self-repair strategy that is mechanically driven may inspire biomimetic materials and technologies that aim to self-repair functional geometries, without regenerating precise shapes and forms.

Materials and Methods

ASW. ASW, 32 ppt, was prepared from Instant Ocean mix using deionized water. For experiments in Fig. 5, magnesium-free ASW was made using recipe 4 in table 3A in the Marine Biological Laboratory Recipe Book (70) and was mixed with regular ASW from the same recipe book to vary magnesium concentration.

Jellyfish Nursery. *Aurelia aurita* polyps were obtained from the Cabrillo Marine Aquarium (San Pedro, CA) and strobilated in the laboratory. Polyps, ephyrae, and medusae were reared at 54 °F in Kreisel tanks (Midwater Systems and ones we built in the laboratory). The colony was fed daily with brine shrimps (*Artremia nauplii*) enriched with *Nannochloropsis* algae. Polyps were occasionally fed L-type rotifers (*Brachionus plicatilis*). To induce strobilation, we used temperature or chemical induction. For temperature-induced strobilation, polyps growing at 54 °F were moved to 68 °F for 2–3 wk, and then returned to 54 °F. Strobilation typically occurred 2–3 wk after. For chemical-induced strobilation, we used the recent finding in ref. 72. Polyps were incubated in 50 mM 5-methoxy-2-methyl-indole (Sigma; M15451) at 68 °F and replaced daily. Strobilation typically occurred 1 wk after. *Chrysaora pacifica*, *Mastigas* sp., and *Cotylorhiza* sp. polyps were obtained from the Monterey Bay Aquarium (Monterey, CA). *C. pacifica* was reared at 54 °F, and the other species at 68 °F. *C. pacifica* and *Mastigias* sp. strobilation happened naturally in the laboratory. Strobilation in *Cotylorhiza* sp. was induced using 50 mM 5-methoxy-2-methyl-indole at 68 °F.

Amputations were performed using a single-edged industrial razor blade. Ephyrae were anesthetized using 0.08% MS-222 or 400 μM menthol. Each ephyra was anesthetized for 2–5 min, amputated, and then returned to ASW. Recovering ephyrae were maintained in an HAG rotator (FinePCR), altered to continually rotate 50-mL Falcon tubes at 7–10 rpm. Ten to 20 ephyrae were placed in each tube. Feeding was performed daily unless otherwise noted. For quick chemical screenings, ephyrae were reared in six-well plates.

Treatment with Inhibitors or Activators. For each treatment, we first screened a wide range of doses to determine the effective doses. Ephyrae were amputated, and then placed in ASW with the inhibitor or activator, at the concentration indicated below. Solutions were changed daily. Ephyrae were tracked between 4 and 14 d. Ephyrae were not fed during the treatment, and we confirmed that starved ephyrae symmetrized at the same rate as fed ephyrae. Specifically, hydroxyurea (Sigma; H8627) was used at 20 μM, 5-fluorouracil (Sigma; F6627) at 10 μM, Z-vad-fmk (APExBIO; A1902) at 100 μM, gambogic acid (Sigma; G8171) at 100 nM, menthol (Sigma; M2772) at 80–400 μM, cytochalasin D (Sigma; C8278) at 500 nM to 2 μM, dihydrocytochalasin B (Sigma; D1641) at 750 nM, latrunculin A (Sigma; L5168) at 60 nM, BTS (Millipore; 203895) at 150 μM, and BDM (Sigma; B0753) at 25 mM.

Staining Protocol. All steps were performed at room temperature, unless indicated otherwise. Nuclei were stained using Hoechst 33342 (Sigma; B2261) at 1:10 concentration, and 30-min incubation in the dark. For costaining, Hoechst staining was done at the end of the procedure before imaging.

Actin was stained using Alexa Fluor 488 Phalloidin (Life Technologies; A12379) at 1:20 concentration. Ephyrae were first anesthetized. This step ensured that the ephyrae would not curl when they were fixed. Ephyrae were next fixed in 3.7% (vol/vol) formaldehyde for 15 min, washed in PBS, permeabilized in 0.5% Triton/PBS for 5 min, washed in PBS, and then blocked using 3% (wt/vol) BSA for 1–2 min. Ephyrae were then incubated in 1:20 phalloidin solution (in PBS) for 1–2 h in the dark, washed in PBS, and imaged.

Dead cells were stained using Sytox Orange (Life Technologies; S34861). Ephyrae were incubated in 1:1,000 Sytox solution (in ASW) for 30 min in the dark at room temperature, and then thoroughly washed with ASW and immediately imaged.

Proliferating cells were stained using Click EdU Alexa Fluor 594 (Life Technologies; C10339) according to the protocol, with the following modifications: Ephyrae were incubated in 15 mL of 1:1,000 EdU in ASW, in the dark, for 24–96 h. In the following steps, a total volume of 10 mL was used in each step. Ephyrae were washed in ASW for 1 h, fixed in 3.7% (vol/vol) formaldehyde/PBS for 15 min, washed in PBS, blocked with 3% (wt/vol) BSA/PBS, permeabilized in 0.5% Triton X-100/PBS for 20 min, and washed in PBS. Ephyrae were then placed in 500 μL of the Click-iT reaction mixture, incubated for 30 min in the dark, followed by washes, and were immediately imaged.

Except for Sytox, all stained ephyrae could be stored in PBS at 4 °C in the dark, for at least 2 wk without significant loss in signal.

Imaging. Dark-field, bright-field, and fluorescent ephyrae were imaged using the Zeiss AxioZoom.V16 stereo zoom microscope equipped with an AxioCam HR 13-megapixel camera, and processed using the Zen software. Optical sectioning of the thick samples and removal of out-of-focus light scattering were performed using the ApoTome.2 module. To facilitate imaging, ephyrae were typically imaged anesthetized in MS-222 or menthol. Coverslips were sometime used to hold ephyrae in place for better image quality. Movies were captured using CamStudio.

Allometry Measurement and Age Correction. For each data point, at least three ephyrae were measured. For every ephyra, the body diameter and three arm lengths were measured. Body diameter was measured by fitting a circle to the body (Fig. 6). Arms were measured to the intersection of the body and the arm. Ephyrae increase in size over time. To account for this, we characterized the growth in body diameter with age. With this correlation, we normalized all measurements to 1-d-old ephyrae.

Ephyrae Grafting. To generate grafted ephyrae, ephyrae segments must heal together. This was achieved by pinning the ephyrae segments next to each other and allowing them to heal together for ~12 h. Ephyrae were pinned on 10-mL Petri dishes filled halfway with 1% agarose/ASW. These dishes were allowed to cool and were then filled with ASW. A donor ephyrae was anesthetized in 400 μM menthol in ASW, and arms were amputated and stored in menthol ASW until grafting. Host ephyrae were then halved in menthol ASW to produce nonsymmetrical tetramer ephyrae. The host ephyrae were then pinned on an agarose dish, to which an arm was then pinned. Pinning was accomplished using cactus spines from *Espostoa mirabilis*. Ephyrae were kept pinned overnight (~12 h) in ASW. The next day, they were unpinned and allowed to recover.

Muscle Contraction Modulation. Menthol (Sigma; M2772) was dissolved in ASW to make 20–400 μM working solutions. $MgCl_2$ at 2.5% (wt/vol) was prepared in ASW. Magnesium-free ASW was made using recipe 4 in table 3A in ref. 73 and was diluted in ASW to make 1:1 to 1:10 final working concentrations. Ephyrae were amputated in an anesthetic and maintained in ASW plus inhibitor for 4 d in six-well plates or rotisserie. For recovery experiments, we waited for 4 d, and then ephyrae were moved back to ASW.

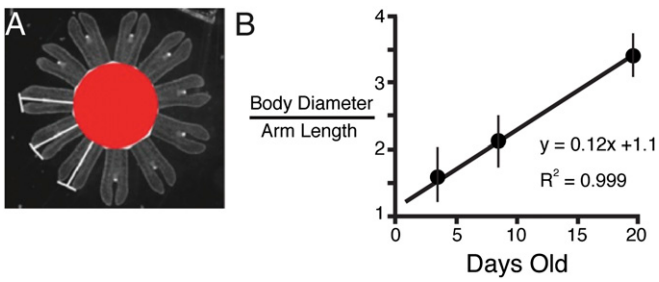

Fig. 6. (*A*) Line indicates arm length. Red area indicates the body. (*B*) Body size increases linearly with age. Error bars were from more than three biological replicates and technical replicates.

ACKNOWLEDGMENTS. We thank the Cabrillo Marine Aquarium and Monterey Bay Aquarium for supplying jellyfish polyps, and especially K. Darrow and W. Patry for their advice on jellyfish nursery. We thank N. Andrew for critical comments that led us to conceiving the pulsation modulation experiment, J. Dabiri for discussions throughout the study, J. Nawroth for pointing us to cactus spines, and E. Meyerowitz for pointing out the importance of viscous ratchet. We thank M. Elowitz, B. Hay, J. H. Cho, C. Frick, H. Nunns, N. Olsman, J. T. Abrams, and B. G. Abrams for suggestions and comments on the manuscript. This work was supported by the National Science Foundation Graduate Research Fellowship Program (to M.J.A.).

1. Graham WM, Kroutil RM (2001) Size-based prey selectivity and dietary shifts in the jellyfish, *Aurelia aurita*. *J Plankton Res* 23(1):67–74.
2. Purcell JEC, Graham WMC, Dumont HJC (2001) *Jellyfish Blooms: Ecological and Societal Importance. Proceedings of the International Conference on Jellyfish Blooms, held in Gulf Shores, Alabama, 12–14 January, 2000.* Hydrobiologia (Springer Science and Business Media, Dordrecht, The Netherlands), Vol 451, p 2001.
3. Olesen NJ, Riisgård HU (1994) Population dynamic, growth and energetics of jellyfish, *Aurelia aurita*, in a shallow fjord. *Mar Ecol Prog Ser* 105:9–18.
4. Lucas CH (2001) Reproduction and life history strategies of the common jellyfish, *Aurelia aurita*, in relation to its ambient environment. *Hydrobiologia* 451(1-3):229–246.
5. Conley K, Uye SI (2015) Effects of hyposalinity on survival and settlement of moon jellyfish (*Aurelia aurita*) planulae. *J Exp Mar Biol Ecol* 462:14–19.
6. Schroth W, Jarms G, Streit B, Schierwater B (2002) Speciation and phylogeography in the cosmopolitan marine moon jelly, *Aurelia* sp. *BMC Evol Biol* 2(1):1.
7. Almeda R, et al. (2013) Effects of crude oil exposure on bioaccumulation of polycyclic aromatic hydrocarbons and survival of adult and larval stages of gelatinous zooplankton. *PLoS One* 8(10):e74476.
8. Winans AK, Purcell JE (2010) Effects of pH on asexual reproduction and statolith formation of the scyphozoan, *Aurelia labiata*. *Hydrobiologia* 645(1):39–52.
9. Thuesen EV, et al. (2005) Intragel oxygen promotes hypoxia tolerance of scyphomedusae. *J Exp Biol* 208(Pt 13):2475–2482.
10. Miyake H, Iwao K, Kakinuma Y (1997) Life history and environment of *Aurelia aurita*. *South Pacific Study* 17(2):273–285.
11. Richardson AJ, Bakun A, Hays GC, Gibbons MJ (2009) The jellyfish joyride: Causes, consequences and management responses to a more gelatinous future. *Trends Ecol Evol* 24(6):312–322.
12. Pitt KA, Lucas CH, eds (2014) *Jellyfish Blooms* (Springer, Dordrecht, The Netherlands).
13. Brusca RC, Brusca GJ (1990) *Invertebrates* (Sinauer Associates, Sunderland, MA), Vol 2.
14. Arai MN (1997) *A Functional Biology of Scyphozoa* (Springer, London).
15. Fu Z, Shibata M, Makabe R, Ikeda H, Uye SI (2014) Body size reduction under starvation, and the point of no return, in ephyrae of the moon jellyfish *Aurelia aurita*. *Mar Ecol Prog Ser* 510:255–263.
16. Lindsay SM (2010) Frequency of injury and the ecology of regeneration in marine benthic invertebrates. *Integr Comp Biol* 50(4):479–493.
17. Pauly D, Graham W, Libralato S, Morissette L, Palomares MD (2009) Jellyfish in ecosystems, online databases, and ecosystem models. *Hydrobiologia* 616(1):67–85.
18. Arai MN (2005) Predation on pelagic coelenterates: A review. *J Mar Biol Assoc U K* 85(03):523–536.
19. Fautin DG, Fitt WK (1991) A jellyfish-eating sea anemone (Cnidaria, Actiniaria) from Palau: *Entacmaea medusivora* sp. nov. *Hydrobiologia* 216(1):453–461.
20. Berryman J (1984) Predation of *Sagartiogeton laceratus* upon *Aurelia aurita* in shallow water. *J Mar Biol Assoc U K* 64(03):725.
21. Cones HN, Haven DS (1969) Distribution of *Chrysaora quinquecirrha* in the York River. *Chesap Sci* 10(2):75–84.
22. Hoppe WF (1988) Growth, regeneration and predation in three species of large coral reef sponges. *Mar Ecol Prog Ser* 50(1):117–125.
23. Hargitt GT (1903) Regeneration in hydromedusae. *Development Genes and Evolution* 17(1):64–91.
24. Stockard CR (1908) Studies on tissue growth. III. An experimental study of the rate of regeneration of *Cassiopea xamachana*. Publication 103 (Carnegie Institution of Washington, Washington, DC).
25. Morgan TH (1901) *Regeneration*. Columbia University Biological Series (Columbia Univ Press, New York), Vol 7, pp 104–106.
26. Chadwick NE, Loya Y (1990) Regeneration after experimental breakage in the solitary reef coral *Fungia granulosa* Klunzinger, 1879. *J Exp Mar Biol Ecol* 142(3):221–234.
27. Schmid V, Alder H (1984) Isolated, mononucleated, striated muscle can undergo pluripotent transdifferentiation and form a complex regenerate. *Cell* 38(3):801–809.
28. Steinberg SN (1963) The regeneration of whole polyps from ectodermal fragments of scyphistoma larvae of *Aurelia aurita*. *Biol Bull* 124(3):337–343.
29. Müller WA, Plickert G, Berking S (1986) Regeneration in Hydrozoa: Distal versus proximal transformation in Hydractinia. *Rouxs Arch Dev Biol* 195(8):513–518.
30. Peebles F (1902) Further experiments in regeneration and grafting of hydroids. *Dev Genes Evol* 14(1):49–64.
31. Morgan TH (1901) Further experiments on the regeneration of Tubularia. *Dev Genes Evol* 13(4):528–544.
32. Laurie-Lesh GE, Corriel R (1973) Scyphistoma regeneration from isolated tentacles in *Aurelia aurita*. *J Mar Biol Assoc U K* 53(04):885–894.
33. Feitl KE, Millett AF, Colin SP, Dabiri JO, Costello JH (2009) Functional morphology and fluid interactions during early development of the scyphomedusa *Aurelia aurita*. *Biol Bull* 217(3):283–291.
34. Sullivan BK, Suchman CL, Costello JH (1997) Mechanics of prey selection by ephyrae of the scyphomedusa *Aurelia aurita*. *Mar Biol* 130(2):213–222.
35. Higgins JE, 3rd, Ford MD, Costello JH (2008) Transitions in morphology, nematocyst distribution, fluid motions, and prey capture during development of the scyphomedusa *Cyanea capillata*. *Biol Bull* 214(1):29–41.
36. Gambini C, Abou B, Ponton A, Cornelissen AJ (2012) Micro- and macrorheology of jellyfish extracellular matrix. *Biophys J* 102(1):1–9.
37. Browne ET (1895) On the variation of the tentaculocysts of Aurelia aurita. *Q J Microsc Sci* 37:245–251.
38. Browne ET (1901) Variation in *Aurelia aurita*. *Biometrika* 1(1):90–108.
39. Mayer AG (1910) *Medusae of the World: The Scyphomedusae* (Carnegie Institute of Washington, Washington, DC).
40. Holst S (2012) Morphology and development of benthic and pelagic life stages of North Sea jellyfish (Scyphozoa, Cnidaria) with special emphasis on the identification of ephyra stages. *Mar Biol* 159(12):2707–2722.
41. Bateson W (1894) *Materials for the Study of Variation* (Macmillan, London).
42. Gershwin LA (1999) Clonal and population variation in jellyfish symmetry. *J Mar Biol Assoc U K* 79(06):993–1000.
43. Mao Y, et al. (2013) Differential proliferation rates generate patterns of mechanical tension that orient tissue growth. *EMBO J* 32(21):2790–2803.
44. Johnson AW, Harley BA (2011) *Mechanobiology of Cell-Cell and Cell-Matrix Interactions* (Springer, New York), pp 62–63.
45. Salic A, Mitchison TJ (2008) A chemical method for fast and sensitive detection of DNA synthesis in vivo. *Proc Natl Acad Sci USA* 105(7):2415–2420.
46. Teng X, Toyama Y (2011) Apoptotic force: Active mechanical function of cell death during morphogenesis. *Dev Growth Differ* 53(2):269–276.
47. Matsuno A (1983) An electron microscopic study on the development of cross-straited muscles in ephyrae of *Aurelia aurita*. *Zoological Magazine* 92(3):416–422.
48. Steinmetz PR, et al. (2012) Independent evolution of striated muscles in cnidarians and bilaterians. *Nature* 487(7406):231–234.
49. Nawroth JC, et al. (2012) A tissue-engineered jellyfish with biomimetic propulsion. *Nat Biotechnol* 30(8):792–797.
50. Heisenberg CP, Bellaïche Y (2013) Forces in tissue morphogenesis and patterning. *Cell* 153(5):948–962.
51. Marston DJ, Goldstein B (2006) Actin-based forces driving embryonic morphogenesis in *Caenorhabditis elegans*. *Curr Opin Genet Dev* 16(4):392–398.
52. Gladfelter WB (1972) Structure and function of the locomotory system of the Scyphomedusa *Cyanea capillata*. *Mar Biol* 14(2):150–160.
53. Nakanishi N, Hartenstein V, Jacobs DK (2009) Development of the rhopalial nervous system in *Aurelia* sp.1 (Cnidaria, Scyphozoa). *Dev Genes Evol* 219(6):301–317.
54. Blanquet RS, Riordan GP (1981) An ultrastructural study of the subumbrellar musculature and desmosomal complexes of *Cassiopea xamachana* (Cnidaria: Scyphozoa). *Trans Am Microsc Soc* 100(2):109–119.
55. Norton JH, Dashorst M, Lansky TM, Mayer RJ (1996) An evaluation of some relaxants for use with pearl oysters. *Aquaculture* 144(1):39–52.
56. Gillary HL (1983) Electrical potentials from the regenerating eye of *Strombus*. *J Exp Biol* 107(1):293–310.
57. Gaudioso C, Hao J, Martin-Eauclaire MF, Gabriac M, Delmas P (2012) Menthol pain relief through cumulative inactivation of voltage-gated sodium channels. *Pain* 153(2):473–484.
58. Fawcett WJ, Haxby EJ, Male DA (1999) Magnesium: Physiology and pharmacology. *Br J Anaesth* 83(2):302–320.
59. Gemmell BJ, et al. (2013) Passive energy recapture in jellyfish contributes to propulsive advantage over other metazoans. *Proc Natl Acad Sci USA* 110(44):17904–17909.
60. Dabiri JO, Gharib M, Colin SP, Costello JH (2005) Vortex motion in the ocean: In situ visualization of jellyfish swimming and feeding flows. *Phys Fluids* 17(9):91108.
61. Megill WM, Gosline JM, Blake RW (2005) The modulus of elasticity of fibrillin-containing elastic fibres in the mesoglea of the hydromedusa *Polyorchis penicillatus*. *J Exp Biol* 208(Pt 20):3819–3834.
62. Schwab WE (1977) The ontogeny of swimming behavior in the scyphozoan, *Aurelia aurita*. I. Electrophysiological analysis. *Biol Bull* 152(2):233–250.
63. Cheung TH, et al. (2012) Maintenance of muscle stem-cell quiescence by microRNA-489. *Nature* 482(7386):524–528.
64. Higuchi H, Takemori S (1989) Butanedione monoxime suppresses contraction and ATPase activity of rabbit skeletal muscle. *J Biochem* 105(4):638–643.
65. Agata K, Saito Y, Nakajima E (2007) Unifying principles of regeneration I: Epimorphosis versus morphallaxis. *Dev Growth Differ* 49(2):73–78.
66. Reddien PW, Sánchez Alvarado A (2004) Fundamentals of planarian regeneration. *Annu Rev Cell Dev Biol* 20:725–757.
67. Wittlieb J, Khalturin K, Lohmann JU, Anton-Erxleben F, Bosch TC (2006) Transgenic Hydra allow in vivo tracking of individual stem cells during morphogenesis. *Proc Natl Acad Sci USA* 103(16):6208–6211.
68. Alexander RM (1964) Visco-elastic properties of the mesogloea of jellyfish. *J Exp Biol* 41(2):363–369.
69. Demont ME, Gosline JM (1988) Mechanics of jet propulsion in the hydromedusan jellyfish, *Polyorchis penicillatus*: II. Energetics of the jet cycle. *J Exp Biol* 134(1):333–345.
70. Hargitt CW (1897) Recent Experiments on Regeneration. *Zool Bull* 1(1):27–34.
71. Coonfield BR (1936) Regeneration in *Mnemiopsis leidyi*, Agassiz. *Biol Bull* 71(3):421–428.
72. Fuchs B, et al. (2014) Regulation of polyp-to-jellyfish transition in *Aurelia aurita*. *Curr Biol* 24(3):263–273.
73. Marine Biological Laboratory, *Biological Bulletin Compendia*. Artifical Seawaters-Recipes. Table 3a, Recipe 4. Available at hermes.mbl.edu/BiologicalBulletin/COMPENDIUM/CompTab3.html#3. Accessed February 4, 2015.